Electronic Supplementary Material (ESI) for Soft Matter.


# SUPPLEMENTAL MATERIAL FOR

## Control of Liquid Crystals Combining Surface Acoustic Waves, Nematic Flows, and Microfluidic Confinement

Gustavo A. Vásquez-Montoya, Tadej Emeršič, Noe Atzin, Antonio Tavera-Vázquez, Ali Mozaffari, Rui Zhang, Orlando Guzmán, Alexey Snezhko, Paul F. Nealey, Juan J. de Pablo*

**This PDF file includes:**

**Other Supplementary Material for this manuscript includes the following:**

- Movie S1 (.mp4 format). Formation of white stripe patterns by applying an RF signal of 15 mW.
- Movie S2 (.mp4 format). Formation of color stripe patterns by applying an RF signal of 20 mW.
- Movie S3 (.mp4 format). The formation of brown stripe patterns by applying an RF signal of 30 mW.
- Movie S4 (.mp4 format). The formation of dynamic behavior of spatially periodic patterns by applying an RF signal of 45 mW.
- Movie S5 (.mp4 format). The formation of a turbulent-like flow behavior by applying an RF signal of 95 mW.
- Movie S6 (.mp4 format). The formation of a turbulent-like flow behavior by applying an RF signal of 130 mW.
- Movie S7 (.mp4 format). The formation of a turbulent-like flow behavior with stripes by applying an RF signal of 260 mW.
- Movie S8 (.mp4 format). The formation of a turbulent-like flow behavior with stripes by applying an RF signal of 320 mW.
- Movie S9 (.mp4 format). Transition to an isotropic phase by applying an RF signal of 400 mW.
- Movie S10 (.mp4 format). In the flow with $Er$ = 3, the SSAW with $R_s = 0.1*10^{-12}$ is switched on and then switched off.
- Movie S11 (.mp4 format). In the flow with $Er$ = 3, the SSAW with $R_s = 0.3*10^{-12}$ is switched on and then switched off.
- Movie S12 (.mp4 format). In the flow with $Er$ = 6, the SSAW with $R_s = 0.1*10^{-12}$ is switched on and then switched off.
- Movie S13 (.mp4 format). In the flow with $Er$ = 6, the SSAW with $R_s = 0.3*10^{-12}$ is switched on and then switched off.
- Movie S14 (.mp4 format). In the flow with $Er$ = 12, the SSAW with $R_s = 0.1*10^{-12}$ is switched on and then switched off.
- Movie S15 (.mp4 format). In the flow with $Er$ = 12, the SSAW with $R_s = 0.3*10^{-12}$ is switched on and then switched off.
- Movie S16 (.mp4 format). First, the SSAW with $R_s = 11.2*10^{-12}$ is switched on without pressure-driven flow. Afterward, while maintaining the SSAW constant, a pressure-driven flow is applied with $Er$ increasing from 0 to 50.

## 1. Continuum simulations

Continuum simulations are based on the Landau-de Gennes (LdG) formalism[1], where the free energy is a function of the tensorial order parameter **Q**

$$\mathbf{Q} = S(\mathbf{nn} - \mathbf{I}/3) \quad (1)$$

In Eq. (1), *S* is the maximum eigenvalue of **Q** and **n** is the eigenvector associated with *S*. The total free energy of the NLC is defined as

$$F = \int_V (f_{\mathrm{LdG}} + f_{\mathrm{el}} + f_{\mathrm{A}})\mathrm{d}V + \int_{\partial V} f_{\mathrm{surf}}\,\mathrm{d}S \quad (2)$$

where $f_{\mathrm{LdG}}$ is the short-range free energy, $f_{\mathrm{el}}$ is the long-range elastic energy, $f_{\mathrm{A}}$ is the acoustic energy, and $f_{\mathrm{surf}}$ is the surface free energy due to anchoring. $f_{\mathrm{LdG}}$ is given by[2]

$$f_{\mathrm{LdG}} = \frac{A}{2}\left(1 - \frac{U}{3}\right)\mathrm{Tr}(\mathbf{Q}^2) - \frac{AU}{3}\mathrm{Tr}(\mathbf{Q}^3) + \frac{AU}{4}\left(\mathrm{Tr}(\mathbf{Q}^2)\right)^2 \quad (3)$$

where *A* and *U* are phenomenological parameters and the scalar order parameter in the bulk ($S_{Bulk}$) is determined by $S_{Bulk} = \frac{1}{4} + \frac{3}{4}\sqrt{1 - \frac{3}{8\,\mathrm{U}}}$. By considering one-constant approximation, elastic energy reads[3]

$$f_{\mathrm{el}} = \frac{L}{2}(\boldsymbol{\nabla}\mathbf{Q})^2, \quad (4)$$

where *L* is a single elastic constant. The acoustic energy is considered as follows[4]

$$f_{\mathrm{A}} = \left(\frac{u_2 \rho_o k^2}{\nu^3}\right) I \cos^2(2\,\pi\,\mathrm{x}\,/\lambda_{\mathrm{x}})\ \mathbf{k}\cdot\mathbf{Q}\cdot\mathbf{k}, \quad (5)$$

where **k** is the propagation vector, $I$ is the acoustic intensity, $\nu$ is the kinematic viscosity, $u_2$ a coupling coefficient, and $\lambda_x$ is a wavelength of applied acoustic field. The simulations consider homeotropic anchoring with the free energy implemented through a Rapini-Papoular expression as[5]

$$f_{\mathrm{surf}} = \frac{1}{2}\mathrm{W}_H(\mathbf{Q} - \mathbf{Q}^0)^2 \quad (6)$$

with the surface-preferred tensorial order parameter, $\mathbf{Q}^0 = S_{Bulk}(\boldsymbol{\nu}\boldsymbol{\nu} - \boldsymbol{\delta}/3)$ and normal surface $\boldsymbol{\nu}$. The temporal evolution of **Q** is simulated by a hybrid lattice Boltzmann method that was used to simultaneously solve a Beris-Edwards equation and a momentum equation. The Beris-Edwards equation is given as[6]

$$\left(\frac{\partial}{\partial t} + \mathbf{u}\cdot\boldsymbol{\nabla}\right)\mathbf{Q} - \mathbf{S} = \Gamma\mathbf{H} \quad (7)$$

with Γ as the rotational diffusion constant. The tensor **S** is the generalized advection term written as

$$\mathbf{S} = (\xi\,\mathbf{A} + \mathbf{\Omega}) \cdot \left(\mathbf{Q} + \frac{\mathbf{I}}{3}\right) + \left(\mathbf{Q} + \frac{\mathbf{I}}{3}\right) \cdot (\xi\,\mathbf{A} - \mathbf{\Omega}) - 2\,\xi \left(\mathbf{Q} + \frac{\mathbf{I}}{3}\right)(\mathbf{Q}\colon \nabla \mathbf{u}) \quad (8)$$

where the tensors $\mathbf{A}$ and $\mathbf{\Omega}$ are the symmetric and antisymmetric velocity gradient tensor $\mathbf{\nabla u}$, respectively. The tensor $\mathbf{H}$ is the molecular field defined as

$$\mathbf{H} = -\left(\frac{\delta \mathcal{F}}{\delta\,\mathbf{Q}} - \frac{\mathbf{I}}{3}\,\mathrm{Tr}\left[\frac{\delta\,\mathcal{F}}{\delta\,\mathbf{Q}}\right]\right) \quad (9)$$

The nematic momentum equation is[7]

$$\rho\left(\frac{\partial}{\partial t} + \mathbf{u} \cdot \nabla\right)\,\mathbf{u} = \nabla \cdot \mathbf{\Pi} - \nu\,\mathbf{u} \quad (10)$$

where $\mathbf{\Pi}$ is the asymmetric stress tensor known as

$$\mathbf{\Pi} = 2\eta\mathbf{A} - \mathrm{P}_0\mathbf{I} + 2\xi\left(\mathbf{Q} + \frac{\mathbf{I}}{3}\right)(\mathbf{Q}\colon \mathbf{H}) - \xi\mathbf{H} \cdot \left(\mathbf{Q} + \frac{\mathbf{I}}{3}\right)$$
$$-\xi\left(\mathbf{Q} + \frac{\mathbf{I}}{3}\right) \cdot \mathbf{H} - \nabla\mathbf{Q}\colon \frac{\delta \mathcal{F}}{\delta\,\nabla\mathbf{Q}} + \mathbf{Q} \cdot \mathbf{H} - \mathbf{H} \cdot \mathbf{Q} \quad (11)$$

This hybrid Lattice Boltzmann method uses a D3Q15 grid. The parameters are chosen for an approximation of 5CB with the coherence length ($\xi_N$) as the unit length. Considering one-constant approximation, the elastic constant is $L = 0.1$ with the LdG parameters $A = 0.1$ and $U = 3.0$. The rotational viscosity constant $\Gamma = 0.133775$. The strength of homeotropic anchoring is $\mathrm{W}_H = 0.1$. The intensity of the acoustic field is in the range between $0.000 \leq I \leq 0.020$.

The critical acoustic intensity $\mathrm{I_{crit}}$ is defined as the intensity needed to reorient the director along with the acoustic wave in *zy* plane when the flow is zero ($I = 0.001$). At this value, the acoustic energy is of the order of the elastic energy of the system $f_A \sim f_{el}$ so that

$$I_{crit} \sim -K\left(\frac{\partial Q}{\partial z}\right)^2 \quad (12)$$

The simulations were done in a rectangular box with periodic boundaries condition implemented on $x$ −axis and the number of simulated nodes in the grid is $N_x = 120$, $N_y = 200$, and $N_z = 40$.

## 2. Determination of Streaming Reynolds Number

Following Riley's[8], for a fluid of density $\rho$ and viscosity $\mu$ the Navier-Stokes equation for incompressible flow maybe written as

$$\frac{\partial \mathbf{v}'}{\partial t'} - \mathbf{v}' \times \omega' = -\frac{1}{\rho}\nabla\left(p' + \frac{1}{2}\rho \mathbf{v}'^2\right) + \mathbf{F}' + \nu\nabla^2\mathbf{v}' \qquad (1)$$

Where $p$' denotes pressure, $\mathbf{v}$' denotes the velocity, $\omega' = \nabla \times \mathbf{v}$' the vorticity, $v = \mu/\rho$ the kinematic viscosity, and $\mathbf{F}$' a body force per unit mass. For a dimensionless analysis, we take $a$ as a characteristic length and $F_0$ a characteristic value of the force. with $\zeta$ as the frequency associated with the oscillatory flow so that $U_0 = F_0/\zeta$ is a characteristic velocity of this flow. Then

$$\mathbf{F} = \mathbf{F}'/F_0, \quad \mathbf{x} = \mathbf{x}'/a, \quad t = \zeta t', \quad \mathbf{v} = \mathbf{v}'/U_0, \quad \omega = a\omega'/U_0 \qquad (2)$$

From which we obtain the dimensionless equation for vorticity

$$\frac{\partial \omega}{\partial t} - \epsilon\nabla \times (\mathbf{v} \times \omega) = -\frac{\partial \Phi}{\partial t} + \frac{\epsilon}{R}\nabla^2\omega \qquad (3)$$

Were $-\frac{\partial \Phi}{\partial t} = \nabla \times \mathbf{F}$.

From Eq. (3) we can observe that the oscillatory flow is characterized by two dimensionless parameters: $\varepsilon = U_0/\zeta a$ which is essentially an inverse of the Strouhal number, and $R = U_0 a/v$ a Reynolds number. No streaming induced by an oscillatory body force will occur if the body force isconservative and $R >> 1$. Eq. 3 can be expressed as

$$\frac{\partial \omega}{\partial t} - \epsilon\nabla \times (\mathbf{v} \times \omega) = -\frac{\partial \Phi}{\partial t} + \frac{\epsilon^2}{R_s}\nabla^2\omega \qquad (4)$$

Following the work initiated by Rayleigh, oscillatory flow induces streaming flows because of viscous attenuation close to a solid boundary, commonly associated with situations for which $ka << 1$. Here, $k$ is the wave number and $a$ the characteristic length. For oscillatory flows at high frequencies,

it is assumed that $\varepsilon << 1$. The dimensionless number $R_s = \varepsilon R$ is essentially a Reynolds number based on the velocity $\varepsilon U_0$. Therefore, the magnitude of $R_s$ determines the contribution of the Laplacian of the vorticity in these flows. $R_s$ is commonly known as the streaming Reynolds number, which is used to study the development of streaming flows using acoustic waves in fluids. It relates the forces related to the oscillations and the viscous dissipation forces.

$$R_s = \frac{U_0^2}{\nu\zeta} \tag{5}$$

To estimate the streaming Reynolds number from experimental data we then need the values of the characteristic length a, the kinematic viscosity of the fluid, and a metric of the characteristic velocity of the oscillatory flow. For a square microfluidic channel, the characteristic length of the channel is given by

$$a = (2 * w * h) / (w + h) \tag{6}$$

Where $w$ is the width of the channel and $h$ is the height of the channel that defines the channel cross-section.

In a system using acoustic waves to generate standing acoustic waves in fluids, the value of $U_0$ relates to the amplitude of the pressure waves generated. therefore, for a device that uses interdigitated transducers to create surface acoustic waves, $U_0$ depends on the Voltage applied to the transducers and therefore on the applied power from the radio frequency source. The task now is to connect the applied power and the voltage signal to the velocity of the propagating wave in the fluid. Based on the quasi-static method for non-reflective single-electrode transducers[9], the total wave amplitude that exits the transducer port is defined as

$$\phi_s(\zeta) = \sum_{m=1}^{m} \phi_{sm}(0,\zeta) = VE(\zeta) \sum_{m=1}^{m} \hat{P}_m exp(-jkx_m) \tag{7}$$

Where it is assumed that all variables have harmonic dependance so that they are proportional to $exp(j\zeta t)$. Here V is the applied voltage, M is the total number of electrodes in the transducer, $k = \zeta/\gamma$ is the wavenumber with phase velocity $\gamma$, and $\hat{P}m = 0, 1, 0, 1, 0, 1, ...$, is the electrode polarity for a single-electrode transducer. $E(\zeta)$ here is an element factor, which varies slowly with $\zeta$ and

is often considered to be constant. For a single electrode transducer, the center frequency $\zeta_{s0}$ occurs when the electrode pitch $p_e$ equals $\lambda/2$, giving $\zeta_{s0} = \pi\gamma/p_e$. At this frequency, it is found that $E(\zeta_{s0}) = 1.694j(\Delta\gamma/\gamma)$, getting $E(\zeta) \approx E(\zeta_{s0})$ for frequencies near to $\zeta_{s0}$. Defining an array factor as

$$A(\zeta) = \sum_{m=1}^{m} \hat{P}_m exp(-jkx_m) \qquad (8)$$

Gives $\varphi_s/V = E(\zeta)A(\zeta)$. Of note, the transducer response $H_t(\zeta)$ is defined by the expression[9]

$$H_t(\zeta) = -jE(\zeta)A(\zeta)\sqrt{\zeta W\epsilon_\infty/(\Delta\gamma/\gamma)} \qquad (9)$$

So that the potential of the wave generated can be written as

$$\Phi_s/V = -jH_t(\zeta)\sqrt{(\Delta\gamma/\gamma)/(\zeta W\epsilon_\infty)} \qquad (10)$$

Here, W is the width of the electrode fingers and $\varepsilon_\infty$ is defined as the capacitance of a unit-aperture single electrode transducer per period. When a voltage V is applied, the power absorbed by the transducer is[9]

$$P_a = G_a(\zeta)|V|^2/2 \qquad (11)$$

Where the conductance $G_a(\zeta)$ and the susceptance $B_a(\zeta)$ are part of the parallel elements added to the capacitance $C_t$ to determine the electrical admittance $Y_t(\zeta)$

$$Y_t(\zeta) = G_a(\zeta) + jB_a(\zeta) + j\zeta C_t \qquad (12)$$

The power of a wave with surface potential $\varphi_s$ can be shown to be[9]

$$P_s = \frac{1}{4}\zeta W\epsilon_\infty|\phi_s|^2/(\Delta\gamma/\gamma) \qquad (13)$$

Which leads with Eq. (10) to the simple relation

$$G_a(\zeta) = |H_t(\zeta)|^2 \qquad (14)$$

The fundamental response of a uniform transducer has

$$G_a(\zeta) \approx G_a(\zeta_0)\,[sin\,(X)\,/X]^2 \qquad (15)$$

where $X \equiv N_p\theta = N_p(\zeta - \zeta_0)/\zeta_0$ and $N_p = M/2$ for single-electrode transducers[9]. Now, it can be shown that for single-electrode transducers

$$G_a(\zeta_0) = \alpha\zeta_0\epsilon_\infty W N_p^2(\Delta\gamma/\gamma), \quad \alpha = 2.87 \qquad (16)$$

Therefore, it follows from this development that as $\zeta \rightarrow \zeta_0$

$$P_{s0} = \frac{1}{4}\alpha\zeta_0\epsilon_\infty W N_p^2(\Delta\gamma/\gamma)V^2 \qquad (17)$$

Eq. (16) relates the total voltage applied form the radiofrequency source to the Power of the acoustic wave leaving an interdigitated transducer that is operating at its resonance frequency $\zeta_0$. Assuming, for simplicity, that there are no losses in the system due to diffraction and dampening, we can relate the power of the traveling surface acoustic wave with the acoustic intensity of the leaking surface acoustic wave in the fluid. For the traveling wave within the fluid, we have that the acousticintensity is related to the amplitude of the velocity profile by

$$I = \rho_o c u^2 \qquad (18)$$

Where $\rho_o$ is the fluid density, $c$ is the speed of sound and $u$ is the fluid velocity related to the oscillatory motion of the fluid. Hence, we can relate the Power of the acoustic wave traveling within the fluid with the characteristic velocity through a cross section area $A_o$ by

$$P_f = A_o\rho_o c U_0^2 \qquad (19)$$

If the power of the acoustic wave exiting the transducer is the power of the traveling wave within the fluid $P_s = P_f$ we can then estimate the characteristic velocity of the wave generatedby the single-electrode interdigitated transducer to be

$$U_0^2 \approx \frac{1}{4A_o\rho_o c}\alpha\zeta_0\epsilon_\infty W N_p^2(\Delta\gamma/\gamma)V^2 \qquad (20)$$

Following this treatment, we conclude that the streaming Reynolds number $R_s$ can be estimatedas a function of the voltage applied to the transducers

$$R_s = \chi V^2 \tag{21}$$

were

$$\chi = \frac{\alpha \epsilon_\infty W N_p^2 (\Delta\gamma/\gamma)}{8\nu A_o \rho_o c} \tag{22}$$

Is a constant defined by the properties of the fluid, the dimensions of the microfluidic channel, the piezoelectric properties of the material where the interdigitated transducers are located, and the architecture of the transducers.

## 3. Supplemental figures

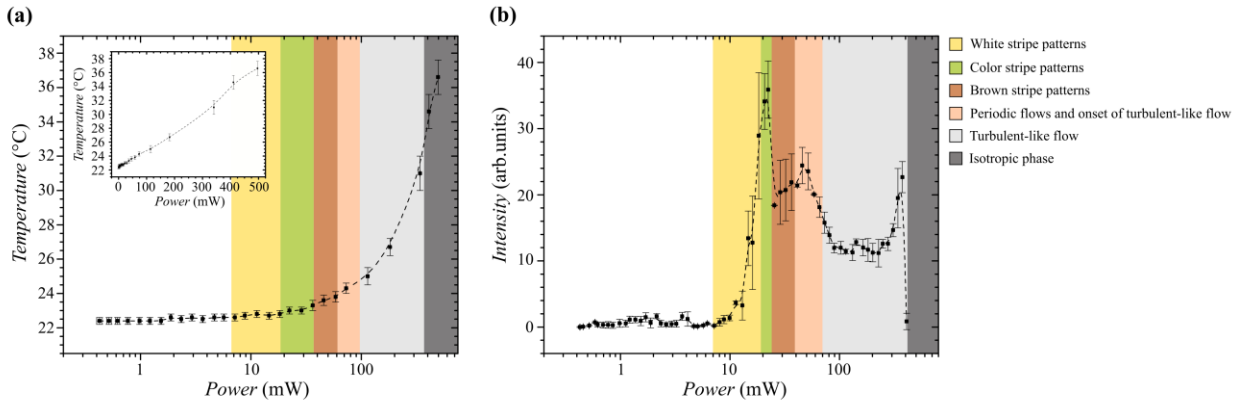


**Fig. S1.** Temperature and transmitted light intensity of NLC under SSAWs. (a) Change in temperature of nematic in a microfluidic channel as a function of input power of RF signal (inset: linear plot). In the region of white and color stripe patterns, the temperature remains relatively stable, whereas the turbulent-like flow regime significantly increases the temperature of the system. (b) The transmitted light intensity obtained from POM images of acoustically induced structures exhibits a peak in the region of color stripe patterns. Colors represent different structure regions (see color legend).

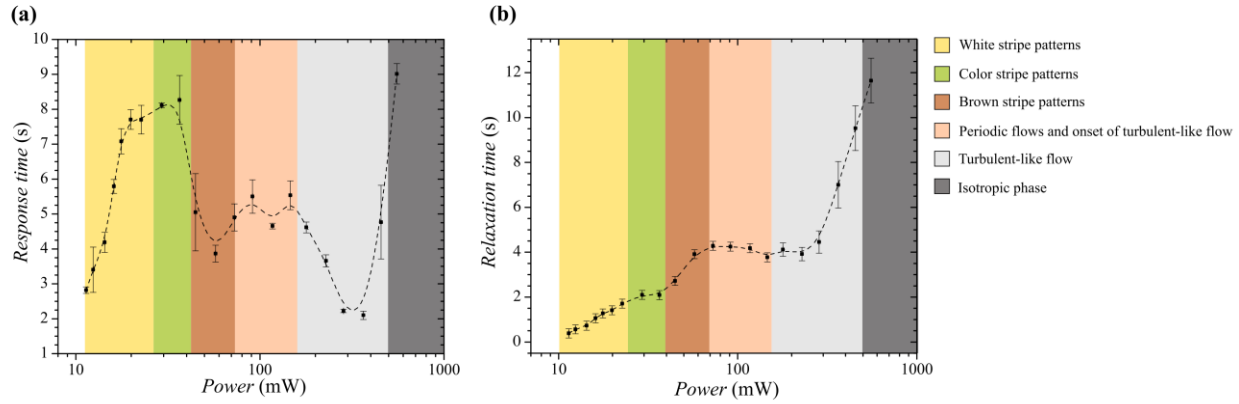


**Fig. S2.** Time scales of acoustically induced structures of NLCs. (a) Response time and (b) relaxation time for nematic to reach a steady state after turning the SSAWs on and off, respectively. Colors represent different structure regions (see color legend).

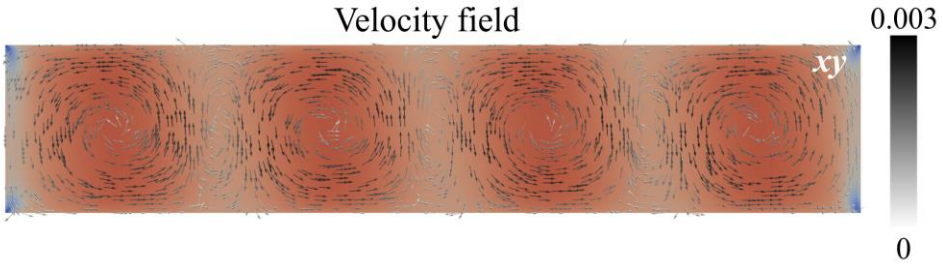


**Fig. S3.** Numerically predicted acoustic streaming flow (represented with black/white arrows) in the microfluidic channel.

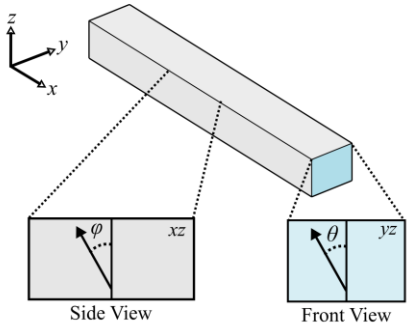


**Fig. S4.** A schematic sketch of the director orientation changes across the microfluidic channel (angle θ) and along the channel (angle φ).

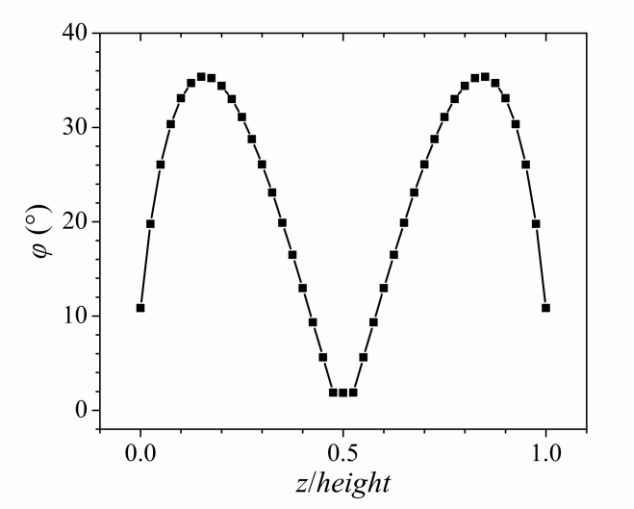


**Fig. S5.** The angle φ of the director field in the dowser state of the weak flow regime through the height of the channel. In the weak flow regime, the nematic molecules bow in the direction of flow, with those closer to the walls bowing more and those in the center of the channel bowing less.

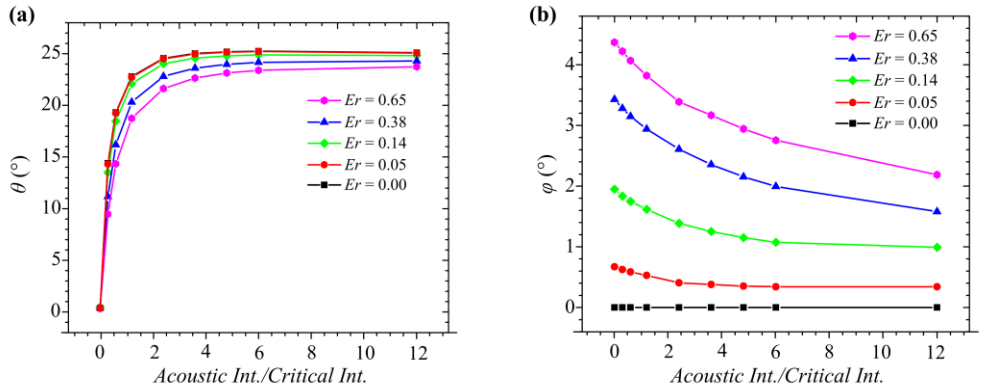


**Fig. S6.** Quantification of the director field angle changes on acoustic pressure nodes across the channel (angle θ) and along the channel (angle φ) the channel at 1/2 of the maximum channel height induced by the acoustic field in the bowser state. (a) Molecules tilt more across the channel at a higher acoustic intensity and less at the same acoustic intensity with a higher nematic flow. (b) A stronger flow bows the molecules more along the channel, while higher acoustic intensity decreases the degree of bowing. Numerical analysis is done in the weak flow regime with *Er* between 0 and 0.65. Note that the scale in simulations is orders of magnitude smaller than that in experiments.

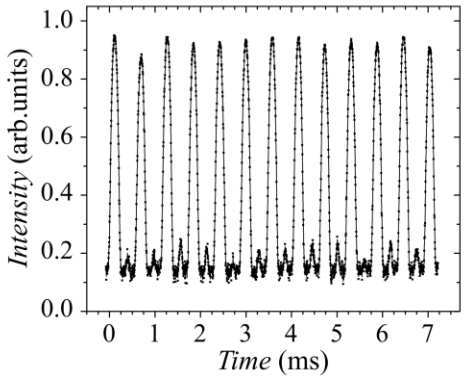


**Fig. S7.** Experiments show that the response times for acoustically induced stripe patterns are in the sub-millisecond regime, for flows in the range of $-5.5 < Er < 5.5$.

## REFERENCES


(1) Chaikin, P. M.; Lubensky, T. C. *Principles of Condensed Matter Physics*; Cambridge University Press: Cambridge, 1995. https://doi.org/DOI: 10.1017/CBO9780511813467.

(2) de Gennes, P. G. *The Physics of Liquid Crystals*; Clarendon Press: Oxford, 1995.

(3) Mori, H.; Gartland, E. C.; Kelly, J. R.; Bos, P. J. Multidimensional Director Modeling Using the Q Tensor Representation in a Liquid Crystal Cell and Its Application to the π Cell with Patterned Electrodes. *Jpn. J. Appl. Phys.* **1999**, *38* (Part 1, No. 1A), 135–146. https://doi.org/10.1143/jjap.38.135.

(4) Selinger, J. V; Spector, M. S.; Greanya, V. A.; Weslowski, B. T.; Shenoy, D. K.; Shashidhar, R. Acoustic Realignment of Nematic Liquid Crystals. *Phys. Rev. E. Stat. Nonlin. Soft Matter Phys.* **2002**, *66* (5 Pt 1), 51708. https://doi.org/10.1103/PhysRevE.66.051708.

(5) Papoular, M.; Rapini, A. Surface Waves in Nematic Liquid Crystals. *Solid State Commun.* **1969**, *7* (22), 1639–1641. https://doi.org/https://doi.org/10.1016/0038-1098(69)90045-3.

(6) Beris, A. N.; Edwards, B. J. *Thermodynamics of Flowing Systems with Internal Microstructure*; Oxford University Press: New York, 1994.

(7) Denniston, C.; Marenduzzo, D.; Orlandini, E.; Yeomans, J. M. Lattice Boltzmann Algorithm for Three-Dimensional Liquid-Crystal Hydrodynamics. *Philos. Trans. Ser. A, Math. Phys. Eng. Sci.* **2004**, *362* (1821), 1745–1754. https://doi.org/10.1098/rsta.2004.1416.

(8) Riley, N. STEADY STREAMING. *Annu. Rev. Fluid Mech.* **2001**, *33* (1), 43–65. https://doi.org/10.1146/annurev.fluid.33.1.43.

(9) Morgan, D. *Surface Acoustic Wave Filters: With Applications to Electronic Communications and Signal Processing*, 2nd Editio.; Academic Press, 2007.